Electron-beam-induced acoustic-wave enhancement of gaseous combustion

S. W. Bidwell, R. A. Bosch,[a] and R. M. Gilgenbach
Intense Energy Beam Interaction Laboratory, Nuclear Engineering Department, The University of Michigan, Ann Arbor, Michigan 48109-2104

(Received 21 July 1988; accepted for publication 3 October 1988)

The combustion rate of premixed gases in a closed vessel was increased by injecting a high-current electron beam into the gas mixture within about 20 ms of spark ignition. This effect was observed with the fuels ethylene, methane, ethane, propane, and *n*-butane. Experimental results provide strong evidence that *e*-beam excitation of the fundamental longitudinal-acoustic mode of the cylindrical chamber is the mechanism of combustion enhancement. An observable combustion enhancement required that the amplitude of the fluid velocity oscillation in this acoustic mode be greater than or approximately equal to the flame propagation speed and was associated with a wrinkled or cellular flame structure with dimensions on the order of $\frac{1}{2}$ cm. These results are in good agreement with values for the threshold acoustic velocity amplitude and dimension of cellular structure predicted for a periodically accelerated flame.

I. INTRODUCTION

A method for increasing the burning rate and ignitability of lean fuel-air mixtures could lead to higher efficiency[1] and decreased pollution[2] in internal combustion engines. Several methods for increasing the burning rate have been explored, including increased gas turbulence,[3] free-radical production,[4] and applying electric fields[5] or microwaves.[6,7] Advanced ignition concepts such as the plasma jet,[8] puff jet,[9] and laser ignition[10,11] have also been pursued.

In a previous paper,[12] we briefly described the influence on ethylene combustion which results from the injection of a high-current electron beam into a closed-vessel explosion initiated by a spark. The flame propagation speed and rate of pressure rise increased by as much as 50%, and the combustion pressure profiles were more reproducible when the electron beam was injected into lean or rich ethylene/air mixtures. The faster combustion was accompanied by an increased level of pressure oscillations,[13] which were audible as a loud squeak.

In this paper we describe detailed experiments on the generation of acoustic waves and enhancement of combustion by electron-beam injection. The enhancement of combustion by *e*-beam injection was observed in the burning of ethylene, methane, ethane, propane, and *n*-butane. Ethylene combustion was enhanced only for lean or rich quiescent mixtures, while the combustion of the remaining gases was enhanced for all values of the equivalence ratio and also in the presence of gas turbulence (flow velocities, ~150 cm/s; turbulence intensities, ~30 cm/s). The results provide strong evidence that *e*-beam excitation of the fundamental longitudinal-acoustic mode of the cylindrical chamber is the mechanism of combustion enhancement. An observable combustion enhancement required that the amplitude of the fluid velocity oscillation in this acoustic mode be greater than or approximately equal to the measured, laboratory frame, flame propagation speed (V_f), and was associated with a wrinkled or cellular flame structure with dimensions on the order of $\frac{1}{2}$ cm. These results are in good agreement with values for the threshold acoustic velocity amplitude and dimension of cellular structure predicted for a periodically accelerated flame.

II. EXPERIMENTAL APPARATUS

The experimental configuration is illustrated in Fig. 1. The experiment consists of a constant-volume combustion bomb attached to an electron-beam generator (Hewlett-Packard Febetron). Electron-beam parameters are $V_p = -400$ kV, $I_p = 1$ kA, and full width pulselength of 300 ns. The electron beam is extracted from a 2.0-cm-diam carbon brush cathode and is injected through a 0.025-mm-thick titanium-anode foil at one end of the combustion chamber. The foil serves the dual purpose of anode and vacuum seal, and is supported by a stainless-steel hibachi structure with 40% transparency so that foil integrity is maintained during the high-pressure (~7-atm) combustion process.

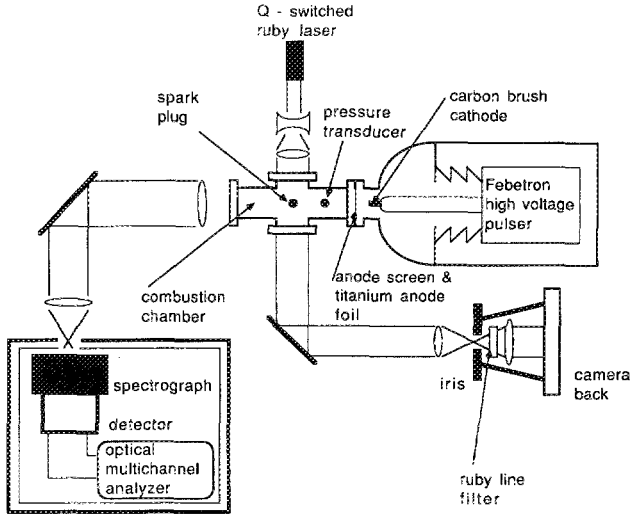

FIG. 1. Experimental configuration.

[a] Present address: KMS Fusion Inc., P.O. Box 1567, Ann Arbor, Michigan 48106-1567.

 0021-8979/89/020782-10$02.40

The aluminum combustion chamber is cylindrical with inside diameter, 8.3 cm; length, 22.2 cm; and volume, 1400 cm^3. The ignitor is a long-reach spark plug and is mounted top and center on the chamber. The ignition system uses conventional automotive ignition components (GM HEI ignition, 12-V automotive battery). There are three fused-quartz windows on the chamber, one on axis on the chamber end and two on the sides for transverse viewing.

Several diagnostics were used to monitor the combustion process. Chamber pressure was measured with an AVL piezoelectric pressure transducer coupled to a Kistler charge amplifier with output to an oscilloscope. The combustion reaction rate was further monitored by viewing OH radical emission with a 307.1-nm bandpass filter and photomultiplier tube mounted at the end of a tube on a side window. The OH radical is an important intermediate specie, and its emission rate is indicative of the overall reaction rate. Two-dimensional resolution of flame front position, shape, and propagation speed was diagnosed by a schlieren photography setup[14] using a pulsed ruby laser and pinhole aperture viewing through the transverse windows. Visible emission spectra were collected using a 1-m spectrograph coupled to a gated optical multichannel analyzer. Not all diagnostics were used concurrently. In addition, Febetron voltage and current were routinely monitored.

III. EXPERIMENTAL PROCEDURE

Essentially, two experiments were performed. One concerns itself with the acoustic waves generated by the electron-beam deposition in the gas and the other with the enhanced combustion rate due to the *e*-beam injection.

In the acoustic investigation, the pressure transducer, recessed about 1 cm from the chamber walls, 8 cm from the anode foil, and shadowed from direct *e*-beam line of sight, records the oscillations produced in the gas. One atm pressure of various inert gases, as well as many combustible mixtures, were introduced into the chamber and their acoustic response studied. At various times small sections of acoustic ceiling tile (USG Acoustic Products) were placed in the chamber windows to serve as acoustic damping. In a given gas, the magnitude of the acoustic disturbance could be changed by varying the Febetron current by means of the charging voltage.

In the combustion investigation, the chamber was evacuated to below 100 mTorr, and oxidant gas (air or O_2), diluent, and fuel were admitted directly into the chamber. The total pressure of the mixtures was 1 atm. To insure proper mixing of the reactants, a small fan agitated the mix for approximately 30 s and was shut off before ignition. Injection of the electron beam into the gas mix preceded (or followed) spark ignition by a preset delay. The beam-influenced combustion was compared with the no-beam case. Ignition of the mixture by the electron beam was never observed, undoubtedly because of the low-energy density deposition of the beam (e.g., in air we estimate $\sim 2\times 10^{-2}$ J/cm^3 near the foil, causing a temperature rise of only ~ 40 °C). As in the acoustic study, the absorbing tile and variations in charging voltage were employed to examine their effect on combustion.

IV. EXPERIMENTAL RESULTS

A. Energy deposition and relaxation

Figure 2 shows a typical voltage and current pulse from the Febetron generator. The top trace shows the voltage on the cathode as monitored by a capacitive divider, the middle trace shows the injected electron current measured with a 6.7-cm-diam brass plate 1 cm from the anode foil in the evacuated combustion chamber, and the bottom trace shows the current collected by the brass plate placed 1 cm from the anode foil in 1 atm of air. The plate is supported by a 1-cm-diam copper tube that extends out of the chamber through a lucite flange. A braided copper strap provides an electrical connection to the combustion chamber, while a wide-band current transformer monitors the beam-collector current. When the chamber is filled with 1 atm air, current striking the plate has two paths to ground, one being a return path through the *e*-beam-produced plasma to the anode and the other along the copper tube. The plasma current accounts for the difference in the copper tube current measured in Figs. 2(b) and 2(c).

The nonuniform energy deposition of the beam was characterized using the brass plate as a beam stop. The brass plate will decrease the bulk gas heating by the amount of *e*-beam energy that would have been deposited in the plate's shadow. Figure 3 shows the beam energy deposition profile as a function of axial position (plate position) in 1 atm air and helium. Following the *e*-beam deposition in the gas and cessation of the resultant acoustic disturbance, the pressure transducer indicates an increase in pressure of several Torr. The displacement in pressure is simply converted to temperature and energy, given the specific heat of the gas. With the plate removed, 2.7 J was deposited in air, while 0.8 J was deposited in helium. It is evident from Fig. 3 that the majority of beam energy is deposited within the first several cm of the gas. Because of the concentrated energy deposition near the foil, visible light emission originates primarily from this region.[15] The *e*-beam-induced light emission dies out within tens of ns after termination of the electron pulse. Spectroscopic studies in an ethylene/Ar/O_2 mixture indicate that a plasma with a temperature of ~ 1.5 eV forms in the region

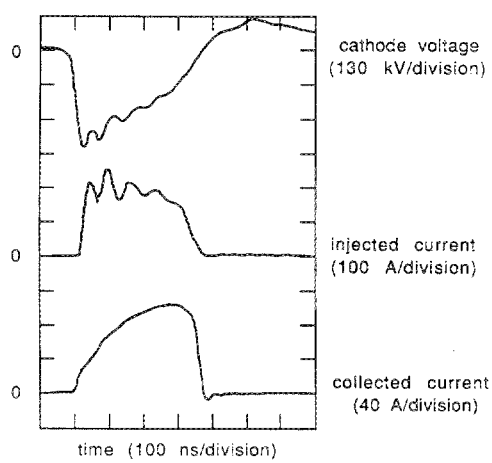

FIG. 2. Cathode voltage, injected current, and collected current for a typical Febetron pulse.

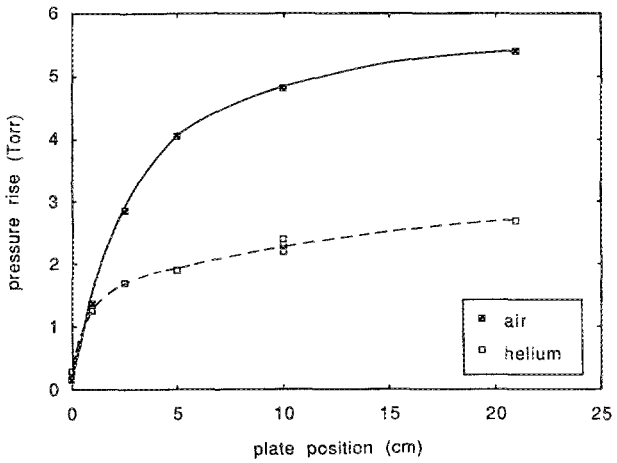

FIG. 3. Axial energy deposition profile in air and in helium at 1 atm pressure, 300 K, using a brass-plate beam stop. For air, 1 Torr pressure rise = 0.46 J. For helium, 1 Torr pressure rise = 0.28 J.

near the foil. Radial variations in energy deposition are not revealed by the plate technique, although placement of thermal-sensitive paper against the anode foil indicated that the majority of the injected electrons are injected within a 1-cm radius of the axis.

B. Acoustic waves

In addition to an overall displacement in pressure, acoustic waves are generated by the inhomogeneity in *e*-beam energy deposition. This is evidenced by the pressure transducer signals shown in Fig. 4 for 1 atm air. Figure 4(a) shows the overall acoustic disturbance from the time of initiation. Figure 4(b) shows the early acoustic oscillations with a frequency of 5.0 kHz discernible—this is in close agreement with the frequency expected for the fundamental radial mode. Figure 4(c) shows the acoustic signal at a later time beginning 21.5 ms after *e*-beam injection. There is clearly a single frequency of 0.8 kHz dominating the spectrum. This dominant frequency is that of the fundamental longitudinal mode which damps out more slowly. Figure 4(d) shows the acoustic signal when a 8.3-cm-diam, 1.3-cm-thick disk of acoustic tile is placed firmly in the end window. Comparing this to Fig. 4(a), one immediately notices the additional damping provided by the tile. When the air was mixed with fuel, in proportions used in the combustion experiments, the acoustic disturbance increased by about a factor of 2 in amplitude.

The mass scaling of *e*-beam-induced acoustics of inert gases at 1 atm was also studied. The envelope of acoustic amplitude for four inert gases is shown in Fig. 5. Sound amplitude increases and the damping rate decreases with increasing gas mass. For xenon the peak amplitude (190 Torr) corresponds to 179 dB. In mixtures of rare gases, O_2, and *n*-butane, the acoustic signal again increased with heavier inert gases.

C. Combustion enhancement

In the combustion study, we investigated five combustible hydrocarbons, four alkanes (methane, ethane, propane,

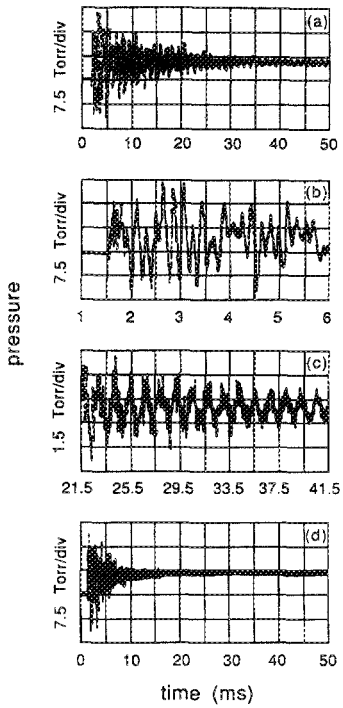

FIG. 4. Electron-beam-produced acoustic waves in 1 atm air. (a) Entire waveform from initiation at time $t = 1.5$ ms with injection of *e* beam. (b) Waveform at early times showing 5.0-kHz P_{10} radial mode. (c) Waveform at later times showing 800-Hz P_{01} longitudinal mode. (d) Entire waveform with acoustic absorber placed in end window.

and *n*-butane) and one alkene (ethylene). Injection of the electron beam into the gas immediately before or after the spark-initiated combustion of these fuels is seen to have a pronounced effect on flame propagation speed, reaction rate, flame front shape, combustion instability, and overall pressure rise.

Figure 6 shows the pressure and OH emission intensity (bandheads at 306.4, 306.7, 307.8, and 308.9 nm)[16] for stoichiometric *n*-butane/air combustion (equivalence ratio $\phi = 1.0$). Figure 6(a) is that for spark-initiated combustion, while Fig. 6(b) shows combustion with the electron beam injected 1 ms before the spark. With the *e*-beam injection, the pressure rise time decreases by 37%, indicating a faster propagation and reaction rate. Hydroxl emission peaks with

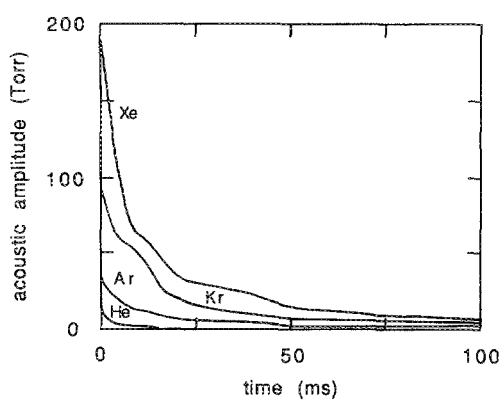

FIG. 5. Acoustic pressure amplitudes for four inert gases at 1 atm pressure and their decay with time.

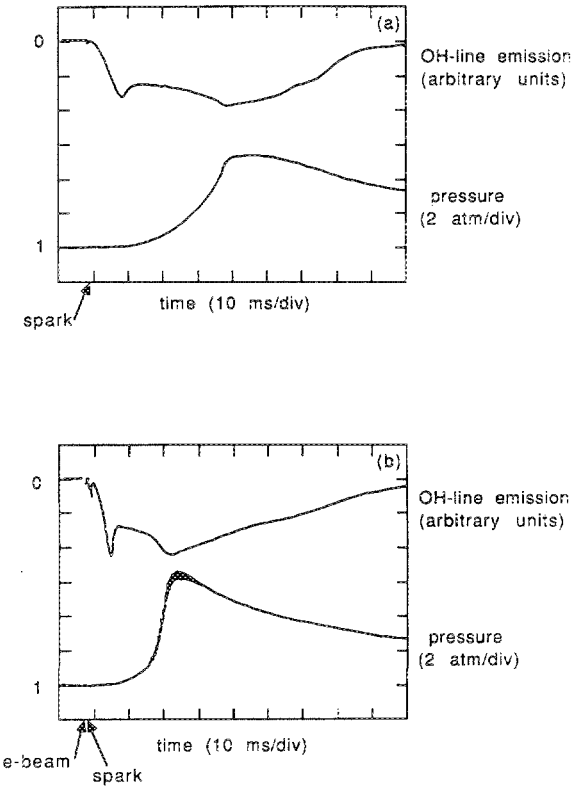

FIG. 6. Combustion of stoichiometric *n*-butane/air at 1 atm pressure. Upper trace: OH-line emission intensity (inverted trace). Lower trace: Pressure transducer signal (2 atm/div). (a) Oscilloscope traces for spark ignition alone. (b) Oscilloscope traces for combustion with *e*-beam injected 1 ms before the spark.

the pressure; this is the familiar phenomenon of afterburning encountered in closed-vessel combustion.[17]

Pressure oscillations indicative of an acoustic instability are apparent in Fig. 6(b). These are acoustic oscillations; their frequency increases with gas temperature ($f \propto T^{1/2}$) and is in agreement with the frequency of the fundamental longitudinal mode of the cylindrical chamber. The pressure oscillations became audible and were heard as a loud squeak or squeal of rising pitch. A microphone placed outside the chamber corroborated the frequency with that measured by the pressure transducer. With a heavier diluent, such as xenon, the sound was heard as a low-frequency chuff. The audible squeak/squeal/chuff proved to be a reliable indicator of *e*-beam effectiveness; a loud sound was invariably accompanied by an increased combustion rate. In the absence of the *e*-beam or with a poor-quality pulse, the sound was much reduced or inaudible and the combustion rate was slower.

The *e*-beam-induced enhancement is seen to have a significant effect over all fuel-air ratios for the alkanes. Figure 7 shows the *n*-butane/air case (*e*-beam injection 1 ms after spark ignition). As was the case with all fuels studied, the most dramatic decreases in rise time are for the rich and lean mixes—mixes in which the reaction rates were slowest. Similar plots were found for the other alkanes. Ethylene showed enhancement for all mixtures except for the most rapid combustions (at stoichiometric conditions).

Except for cases such as stoichiometric ethylene/air where combustion reaction rate was unaffected, peak pressure with *e*-beam-injected combustion was consistently higher. Typical peak pressures were ~5–8 atm, with *e*-beam-injected combustions 10% higher. With a faster reaction rate, there is less heat loss to the chamber, resulting in higher temperatures and pressures (i.e., the combustion approaches an adiabatic process). For example, with lean ethylene/air ($\phi = 0.6$), assuming idealized complete combustion with an energy release of 2970 J, the faster reaction rate should reduce heat loss by 270 J—an improvement of 13%.

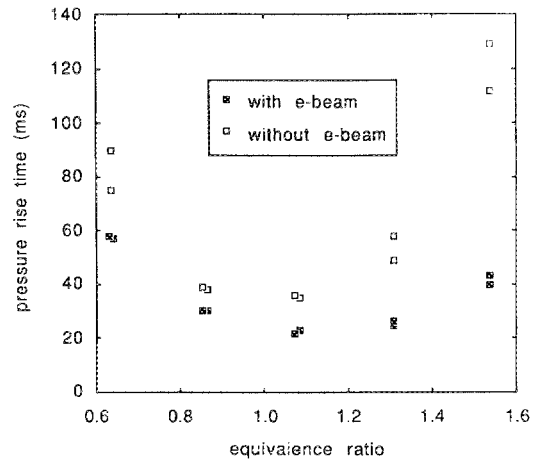

FIG. 7. Pressure rise time (measured from time of spark to pressure peak) in *n*-butane/air as a function of equivalence ratio ϕ. Electron-beam injection occurs 1 ms after spark ignition.

To examine combustion under mildly turbulent conditions, a small fan was placed inside the chamber; it produced gas flow velocities around 150 cm/s and turbulence intensity levels near 30 cm/s as determined by a hot-wire anemometer. In all cases the induced turbulence tends to speed up the combustion. The *e*-beam injection still provides combustion enhancement in the alkanes, even under these turbulent conditions. Figure 8 shows stoichiometric alkane/air combustion under turbulent and nonturbulent conditions with and without the electron beam (*e*-beam injection 1 ms before spark ignition). In the case of turbulent ethylene combustion, no combustion enhancement was observed.

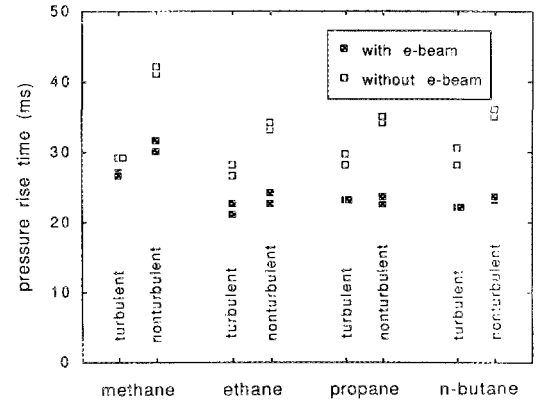

FIG. 8. Pressure rise times for stoichiometric alkane/air mixtures in quiescent and mildly turbulent conditions (flow velocities, ~150 cm/s; turbulence intensities ~30 cm/s). Turbulent conditions produced faster reaction rates and reduced the *e*-beam effect. Electron-beam injection occurs 1 ms before spark ignition.

Schlieren photography utilizing 20-ns pulsed ruby laser illumination allowed the visualization of the flame front and the measurement of its propagation speed. Figure 9 shows the schlieren photographs for the combustion of rich ethylene/Ar/O_2 mixes ($\phi = 2.0$). The photos on the left are for spark-initiated combustion alone, while those on the right are for the *e*-beam injected 1 ms after spark ignition. The spark plug is visible at top center. The *e*-beam-injected combustions show an elliptical front, while the spark-only flame fronts are more spherical. Also evident is the advanced progression of the *e*-beam-injected flames especially in the vertical (transverse to *e*-beam) direction. For the case of *e*-beam injection, the sides of the flame front display a wrinkled or cellular structure which is common to all of the observed *e*-beam-enhanced combustions.

Figure 10 shows the flame front position versus time measurements for rich ethylene/Ar/O_2 ($\phi = 2.0$) combustions, extracted from schlieren photos for the radial direction of propagation. For early times (< 14 ms) the chamber pressure has not risen significantly and the flame progresses in a constant-pressure regime. The flame propagation speed increase resulting from *e*-beam injection in this case is 110% (from 296 to 620 cm/s). For lean ethylene/Ar/O_2 ($\phi = 0.4$) an 84% increase in flame propagation speed is observed. Lean ethylene/air ($\phi = 0.6$) flame propagation speed increased by 50%, while rich ethylene/air ($\phi = 1.7$) flame propagation speed increased by 40%.

By varying the time at which the *e*-beam was injected into the mix relative to the spark plug ignition, the persistence of the effect could be determined. Figure 11 shows such a plot for stoichiometric *n*-butane/air mixes. The combustion is enhanced (sped up) for cases in which the *e*-beam is injected from 20 ms before the spark (-20 ms) all the way to 20 ms after the spark ($+20$ ms). Injecting the *e*-beam in the time frame of -10 to $+10$ ms about the spark has essentially the same effect. Similar plots can be drawn for the other fuels. A significant observation is that the persistence time, when the *e*-beam is injected before the spark, in *n*-butane (18 ms) is larger than any other hydrocarbon investigated. The persistence time in stoichiometric methane/air mixes is only 7 ms. When the diluent xenon is used (stoichiometric *n*-butane/Xe/O_2), the *e*-beam-induced effect persisted for 60 ms. However, when using helium as a diluent it was impossible to get any combustion enhancement whatsoever. The measured persistence times were of the same magnitude as the damping times for the acoustic disturbance generated by the *e* beam.

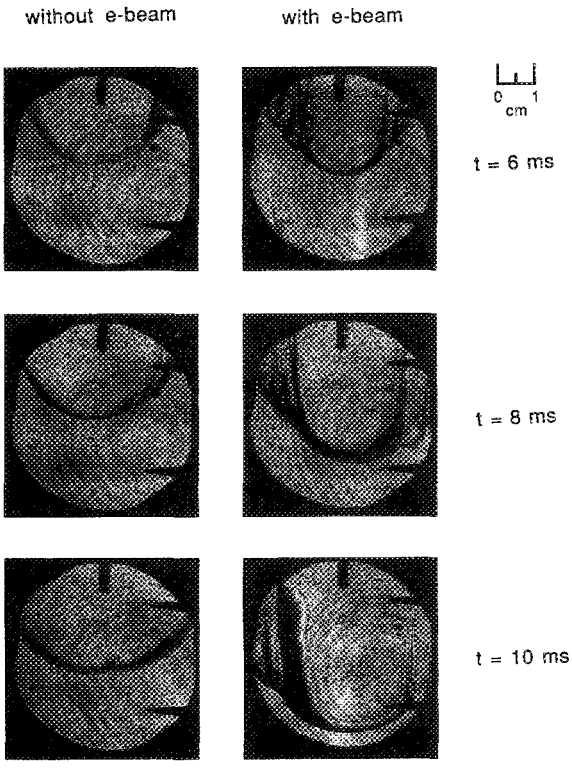

FIG. 9. Schlieren photographs of 1 atm, rich ($\phi = 2.0$) ethylene/Ar/O_2 combustion showing flame front progression with time. Left-hand-side photos show combustion with spark ignition alone, while right-hand-side photos show combustion with electron-beam injection 1 ms after spark ignition. Spark ignition occurs at time $t = 0$. The spark plug is at top center.

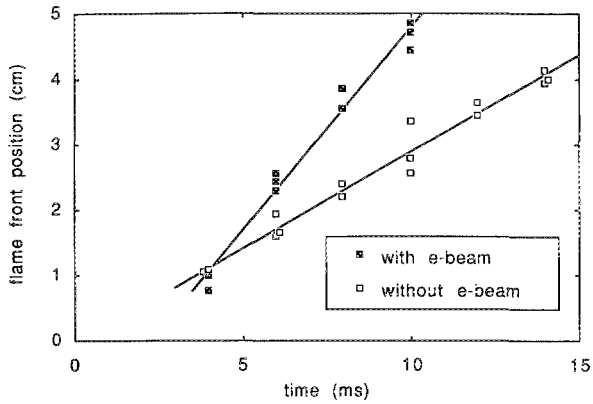

FIG. 10. Flame front position, transverse-to-electron beam direction, measured with laser schlieren photography (from Fig. 9). Data are for rich ethylene/Ar/O_2 combustion ($\phi = 2.0$). From the slope of the lines, the flame propagation speed was determined to be 620 cm/s with electron-beam injection and 296 cm/s without electron-beam injection.

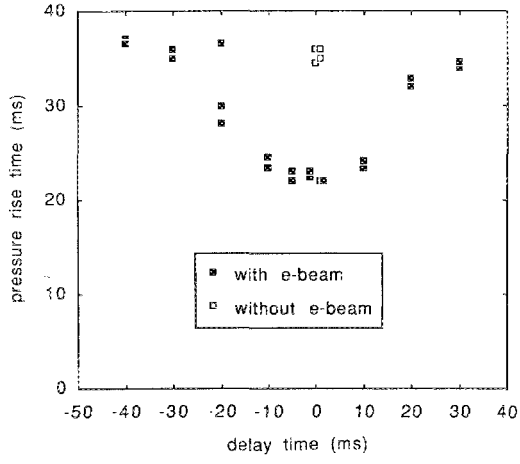

FIG. 11. Pressure rise time as a function of delay time (time of *e*-beam injection relative to spark plug ignition) for stoichiometric *n*-butane/air combustion. The persistence time (20 ms for this mix) is the time at which the *e*-beam enhancement ceases—when the pressure rise time is comparable to the spark-alone case.

The presence of increased acoustic instability in the enhanced combustion, as well as the observation that the persistence time is comparable to the acoustic damping time, suggest that the acoustic waves generated by the e-beam are responsible for the combustion enhancement.

This hypothesis was tested by inserting an acoustic tile into the end window. The presence of the acoustic tile is expected to have little or no effect upon radical formation, excited states, or other chemical reactions initiated by the e beam, while it quickly damps the acoustic disturbance. In all cases studied, the combustion enhancement was eliminated by the presence of the acoustic tile. This provides strong evidence that the acoustic waves are the mechanism of combustion enhancement. The observation of increased acoustic instability in the fundamental longitudinal mode suggests that excitation of this mode by the e beam is responsible for the combustion enhancement.

By varying the injected e-beam energy (by adjusting the Marx generator charging voltage), one could affect the acoustical disturbance produced. The acoustic amplitude increased with the injected e-beam energy. The magnitude of the fundamental longitudinal mode is characterized by its velocity amplitude V_{01} related to the pressure amplitude by $V_{01} = P_{01}/\rho C_s$, where ρ is gas mass density and C_s is sound speed. The pressure transducer was mounted near the center of the chamber and as such measured 0.4 times the pressure amplitude occurring at the chamber ends. Therefore, P_{01}, the fundamental longitudinal pressure amplitude, was found by multiplying the measured amplitude by 2.5. Plotted in Fig. 12 is the pressure rise time versus the acoustic velocity amplitude (fundamental longitudinal mode) for stoichiometric n-butane/air combustion with e-beam injection 1 ms before ignition. There is a clear threshold for combustion enhancement occurring with acoustic velocities about 320 cm/s which corresponds to the flame propagation speed in this combustion. Further increases in the acoustic amplitude produced faster rise times, and a possible saturation of enhancement may occur at larger amplitudes. The upper velocity amplitude was limited by the output of the Febetron generator.

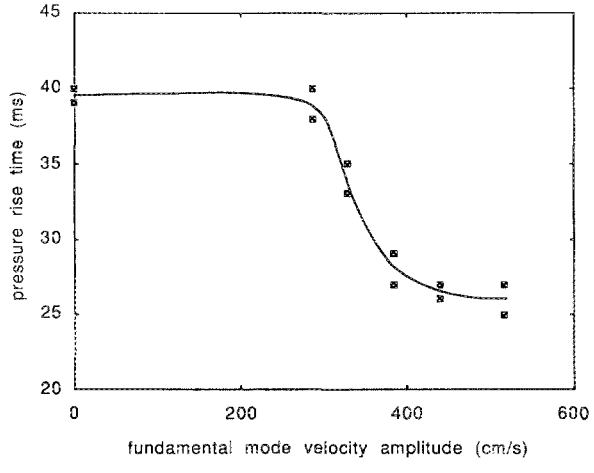

FIG. 12. Pressure rise time as a function of fundamental longitudinal mode velocity amplitude (V_{01}) for stoichiometric n-butane/air combustion. A threshold at $V_{01} \simeq 320$ cm/s is apparent—this velocity is approximately the flame propagation speed for spark-alone combustion.

The acoustic threshold indicated by Fig. 12 is examined for a variety of fuel-oxidant mixtures in Table I. The threshold is examined by noting the persistence time t_p for each mixture: the longest period of time before spark ignition for which the e beam can be injected and enhancement observed. From the acoustic data gathered on these mixtures, we measured the fundamental longitudinal pressure amplitude at time t_p following e-beam injection. The minimum pressure amplitude necessary for combustion enhancement, P_{01}^{th}, was found by multiplying the measured amplitude at $t = t_p$ by 2.5. The corresponding threshold acoustic velocity amplitude, V_{01}^{th} is calculated from P_{01}^{th} as before: $V_{01}^{th} = P_{01}^{th}/\rho C_s$. The pressure rise times in Table I were measured directly with the transducer for spark-ignited combustion with no e beam. From the schlieren studies of eight different cases, in which the flame propagation speed varied by more than a factor of 2, it was found that the flame propagation speed in the early, constant-pressure period of the combustion was linearly proportional to the pressure rise time (as expected) and obeyed

$$(V_f)(\text{pressure rise time}) = 11.5 \text{ cm} \pm 10\%.$$

Using this relation, the flame propagation speeds in Table I were derived—except for the ethylene-air combustions, for which the flame propagation speed was determined directly from schlieren photographs. It was found that the threshold acoustic velocity amplitude V_{01}^{th} is comparable to the flame propagation speed. In particular, for the variety of mixtures, the ratio of threshold acoustic velocity amplitude to flame propagation speed is nearly unity. Summarizing, no enhancement of combustion was observed unless the acoustic disturbance generated acoustic velocities in the fundamental

TABLE I. Various fuel-oxidant mixtures with their respective combustion and acoustic characteristics. The persistence time t_p is the longest time preceding spark ignition at which e-beam injection enhances reaction rate. The fundamental longitudinal pressure amplitude threshold P_{01}^{th} is 2.5 times the transducer-measured amplitude at time $t = t_p$ following e-beam injection. The corresponding velocity amplitude threshold, V_{01}^{th} is calculated from the pressure amplitude by $V_{01}^{th} = P_{01}^{th}/\rho C_s$, where ρ is gas mass density and C_s is sound speed. Pressure rise time for spark-alone combustion allowed calculation of flame propagation speed V_f through the relation (V_f) (pressure rise time) = 11.5 cm $\pm$ 10%. Comparison of the acoustic velocity amplitude to the flame propagation speed indicates a threshold condition for reaction rate enhancement near unity (i.e., $V_{01}^{th}/V_f \simeq 1.0$).

Combustible mixture[a]	t_p (ms)	P_{01}^{th} (Torr)	V_{01}^{th} (cm/s)	Pressure rise time (ms)	V_f (cm/s)	V_{01}^{th}/V_f
CH_4/air	7	11	320	41	280	1.1
C_2H_6/air	12	13	380	34	340	1.1
C_3H_8/air	14	13	380	35	330	1.2
n-C_4H_{10}/air	18	11	320	36	320	1.0
C_2H_4/air ($\phi = 0.6$)	11	11	320	44	260	1.2
C_2H_4/air ($\phi = 1.7$)	20	11	320	44	260	1.2
n-C_4H_{10}/Ar/O_2	15	21	540	20	580	0.9
n-C_4H_{10}/Xe/O_2	60	24	350	31	370	0.9

[a] Stoichiometric except where equivalence ratio (ϕ) is noted.

longitudinal mode with amplitude greater than or equal to the flame propagation speed.

The fuel-oxidant mixtures in which no combustion enhancement was observed could be explained by the existence of a threshold acoustic velocity amplitude. For example, in stoichiometric *n*-butane/He/O_2 mixes (not listed in Table I) the flame propagation speed is 720 cm/s, while the greatest acoustic velocity amplitude was only 470 cm/s; as a result, no enhancement in flame propagation speed/combustion rate was ever observed for this mixture. Similarly, stoichiometric ethylene/air mixes and turbulent ethylene/air mixes showed no enhancement since the acoustic velocity amplitude did not exceed the characteristically high flame propagation speed.

Of a related interest was the long-noticed effect of no combustion enhancement when the *e*-beam generator cathode arced and delivered a poor-quality *e*-beam pulse to the mixture. This is explainable by acoustic-wave production—cathode arcs produced decreased acoustic waves and hence lack of enhancement.

V. ANALYSIS AND DISCUSSION

A. Energy deposition and relaxation

Let us consider the sequence of events initiated by the injection of a pulse of electrons into 1 atm of gas. An approximately rectangular electron current pulse (180 A, 350 ns, energy ≈ 10 J) enters the combustion chamber within a 1-cm radius of the chamber axis. During most of the *e*-beam pulse, the electron range in 1 atm of air exceeds 5 cm, so that the electrons can deposit energy throughout the chamber and on the chamber walls. However, during the final 50–100 ns, the electron energy is sufficiently small that the electrons will be stopped within ~ 5 cm of the anode foil.

Visible light emission from a 1-atm gas is primarily emitted from within several cm of the Ti foil,[15] consistent with the concentrated energy deposition in this region. Spectroscopic studies in an ethylene/Ar/O_2 mixture indicate the formation of a plasma with electron temperature of ~ 1.5 eV. The light emission dies out within tens of ns from the termination of the electron pulse, as the population of electronically excited states decreases from collisional deactivation[18] and the lack of electron-impact excitation following electron recombination.[19]

Energy loss through radiation generally comprises a minority of the deposited energy when at least several percent of O_2 or N_2 are present in a 1-atm mixture. This is due to the large rate of collisional quenching of electronically excited states by these molecules.[18,20] Some deposited energy may contribute towards the population of metastable states, radical formation, and radiation chemistry. Within tens of μs, the majority of the remaining energy relaxes into an equilibrium excitation of translational, rotational, and vibrational degrees of freedom,[21,22] leading to a nonuniform heating and pressure rise of the gas on a timescale short compared to the acoustic transit time of the combustion chamber (~ 0.6 ms).

The nonuniform pressure rise generates acoustic waves (the electron-acoustic effect[23]). These waves damp out on a timescale of tens of ms, primarily as a result of absorption when reflecting from the chamber walls,[24] transmitting part of their energy to wall heating. Finally, from the *e*-beam deposition, one is left with a bulk pressure rise which dies out on a timescale of ~ 2 s as heat conduction cools the gas. For 1 atm of air, the observed acoustic waves had a peak amplitude of 15 Torr at the position of the pressure transducer and an estimated energy of 0.02 J, while the bulk pressure rise of 5.4 Torr indicates that 2.5 J of energy remains in the form of bulk heating after the acoustic waves damp out, giving a temperature rise of 2.1 °C.

When the *e*-beam energy is suddenly deposited into a small volume V of the gas-filled chamber, the majority of the energy causes a sudden localized pressure perturbation δP. When this perturbation is small compared to the initial pressure ($\delta P/P \ll 1$), the total deposited energy is $V\delta P/(\gamma - 1)$, and the acoustic energy[25] is $V(\delta P)^2/2\gamma P$, where γ is the ratio of specific heats. For $\delta P/P \ll 1$, the sound energy is a small portion of the total deposited energy ($\sim 1\%$ in this experiment). Consequently, the bulk pressure rise remaining after the sound is absorbed provides a good measurement of the deposited energy.

The measurement of the bulk pressure rise for different positions of the beam collector exploits this fact in order to characterize the longitudinal energy deposition profile. The bottom trace of Fig. 2 shows the current drawn by this plate when placed 1 cm from the Ti foil in 1 atm of air. The measured current does not equal the *e*-beam current incident on the collector because a portion of the *e*-beam current can return to ground through the *e*-beam-created plasma. This current will not be detected by the current transformer which monitors the coaxial current path from the beam collector to ground. The coaxial current path had a calculated inductance L of $\sim 0.15\ \mu$H.

In order to understand this current trace, we note that the collected *e*-beam current can return to the Febetron through the inductance of the coaxial current path L or the impedance Z of the *e*-beam-produced plasma.[26] For a rectangular *e*-beam current pulse and resistive plasma impedance, the current through the inductive path (i.e., the measured current) will rise asymptotically to the *e*-beam current on a timescale $\tau = L/Z$. From Fig. 2, we note that $\tau \sim 100$ ns, so that $Z = L/\tau \approx 1.5\ \Omega$. The energy deposited by the plasma current ($E = \int I^2 Z dt \approx 0.01$ J) is small compared to that deposited by the *e* beam. Thus, the presence of the *e*-beam collector should not greatly modify the amount of energy deposited in the region between the Ti foil and the collector. At the end of the *e*-beam pulse, the current through the inductive path drops quickly to zero, indicating an increased plasma impedance as the electrons quickly recombine. Using the estimated plasma resistivity

$$\rho = ZA/d \approx (1.5\ \Omega)(1.2\times 10^{-3}\ \mathrm{m}^2)/(0.01\ \mathrm{m}) \approx 0.18\ \Omega\ \mathrm{m},$$

electron temperature $T_e \approx 1.5$ eV, and electron-neutral cross section $\sigma \approx 10^{-15}$ cm^2, we employ the relation for the resistivity of a weakly ionized plasma,[27]

$$\rho = (m_e n_n \sigma/n_e e^2)(kT_e/m_e)^{1/2},$$

to estimate that the plasma electron density is $\sim 10^{14}$–10^{15} cm^{-3} during the *e*-beam pulse.

Figure 3 shows the energy deposited by the e-beam (obtained by measuring the bulk pressure rise) as a function of the position of the e-beam collector, for the cases where the chamber was filled with 1 atm air or 1 atm helium. The figure shows that a large proportion of the energy deposition occurs within several cm of the Ti foil, as expected. For 1 atm air, we estimate that a pressure rise of ~ 100 Torr and a temperature rise of ~ 40 °C is present immediately after the e-beam pulse within ~ 2 cm of the center of the Ti foil. This results in an estimated acoustic energy of 0.02 J, in agreement with the value calculated from the measured acoustic-wave amplitudes. In the case of He, the lower cross section for electron-gas interaction results in a decreased energy deposition and a decreased level of acoustic-wave excitation. For fuel-air mixtures, the heavier rare gases Ar, Kr, and Xe, and mixtures of n-butane with O_2 and Ar or Xe, the energy deposition and acoustic excitation exceeded that of air alone. This is expected, since the cross section for the beam-gas interaction increases for larger molecules.

B. Acoustic waves

Since the temperature increase from the energy deposition causes little change in the sound velocity ($\delta C_s/C_s < 6\%$), the pressure disturbance will approximately obey the wave equation

$$[\nabla^2 - (1/C_s^2)\partial_t^2]P = 0.$$

Because the gas is stationary, the initial condition, $\partial_t P|_{t=0} = 0$, follows from the continuity equation

$$\partial_t P \propto \partial_t n = -\nabla \cdot n\mathbf{v} = 0.$$

The boundary condition, $\mathbf{n}\cdot\nabla P \equiv 0$, is approximately obeyed at the nearly rigid walls, where $\mathbf{n}\cdot\mathbf{v} \equiv 0$. These initial and boundary conditions imply that the azimuthally symmetric, time-dependent pressure disturbance in a cylindrical chamber of length L and radius R obeys

$$P(r,z,t) = \sum_{m,n=0}^{\infty} P_{mn} J_0(\gamma_m r/R)\cos(n\pi z/L)\cos(\omega_{mn} t),$$

where

$$\omega_{mn} = C_s[(\gamma_m/R)^2 + (n\pi/L)^2]^{1/2},$$

and γ_m is the mth zero of J_1. ($\gamma_0 = 0$, $\gamma_1 = 3.83$, etc.) The coefficients P_{mn} are uniquely determined by the initial pressure profile $P(r,z,t=0)$. Conversely, a knowledge of the time-dependent pressure $P(r_0,z_0,t)$ at a position on the chamber wall that is not a pressure node can be used to determine $P(r,z,t=0)$ and thus diagnose the energy deposition profile.[28] For 1 atm air in our combustion chamber, the frequencies $f_{10} = \omega_{10}/2\pi$ and $f_{01} = \omega_{01}/2\pi$ are 5.0 and 0.78 kHz, respectively, in close agreement with the observed frequencies of Figs. 4(b) and 4(c).

The attenuation of sound waves will alter the time behavior of this solution. For the nearly rigid metal and quartz surfaces of the combustion chamber and frequencies of ~ 1 kHz, the attenuation of the acoustic waves will primarily result from the imperfect reflections from the walls,[24] and 1%–5% energy absorption may be expected per wall reflection.[29] For $R \ll L$, the modes which reflect off the side walls ($m > 0$) will decay more rapidly as a result of more frequent reflection, while higher frequencies will decay more rapidly as a result of greater absorption per reflection. As a result, the fundamental longitudinal mode is expected to be the dominant mode at large times. This is in agreement with our results of Fig. 4, which show that the acoustic signal is dominated by the fundamental longitudinal mode (800 Hz) after ~ 20 ms. The fundamental longitudinal mode is subsequently damped out with a decay time of ~ 20 ms. The fundamental mode amplitude at the transducer position is ~ 4 Torr when $t = 0$, which implies an amplitude of 10 Torr at the antinodes located at the ends of the chamber. This is in good agreement with the value calculated from the energy deposition profile measured with the brass beam stop (Fig. 2).

The associated fluid velocity amplitude (at the velocity antinode in the center of the chamber) is $V_{01} = P_{01}/\rho C_s$, where P_{01} is the pressure amplitude for the fundamental longitudinal mode, ρ is the gas mass density, and C_s is the sound speed. For the measured amplitude in air immediately following the e-beam pulse, $P_{01} = 10$ Torr, so that $V_{01} = 300$ cm/s. The amplitude of fluid displacement, $X_{01} = V_{01}/\omega_{01}$, is 0.6 mm in the center of the chamber. This displacement is small compared to the distances measured in the schlieren photographs, so that it will cause negligible error in the schlieren photography measurements of the (average) flame propagation speed.

For the heavier rare gases, the acoustic disturbance was larger and damped out more slowly. The larger acoustic disturbance results from the increased beam-gas interaction with larger molecules. The slower decay is expected, since the rate of wall reflection (the primary cause of sound absorption) is reduced because of the lower sound speed.

C. Combustion enhancement

The experimental results demonstrate that e-beam injection produces a significant increase in the rate of combustion. The flame propagation speed and rates of pressure rise and OH emission were increased when a sufficiently large e-beam pulse energy was injected. The faster combustion was accompanied by a wrinkled or cellular flame front and increased level of acoustic instability in the fundamental longitudinal mode of the combustion chamber.

The results provide strong evidence that the mechanism of combustion enhancement was the excitation of the fundamental longitudinal-acoustic mode of the cylindrical combustion chamber. The evidence includes the following: (1) The persistence time of e-beam-enhanced combustion is comparable to the acoustic damping time. (2) The combustion enhancement was eliminated by placing an acoustic tile in the end window of the chamber. This tile quickly damps out acoustic waves, but is expected to have little or no effect upon chemical processes initiated by the e beam. (3) The enhanced combustion was always accompanied by an increased level of acoustic instability in the fundamental longitudinal mode. (4) The observation of combustion enhancement required that the velocity amplitude of the fundamental longitudinal-acoustic mode be greater than or approximately equal to the flame propagation speed at the beginning of combustion.

The feasibility of this mechanism is supported by a large body of experimental and theoretical work which demonstrates increased combustion rates in the presence of acoustical disturbances and the acoustic instability.[30-34]

The approximate equality between the threshold acoustic velocity amplitude required for combustion enhancement and the flame propagation speed strongly suggests that the fluid motion associated with the acoustic waves, and not the direct effect of the pressure perturbation, is the primary cause of combustion enhancement. This is further supported by the wrinkled, cellular flame front in the case of enhanced combustion, which is expected to result from fluid motion and produce more rapid combustion. Furthermore, the schlieren photography showed that the flame propagation speed increased near the spark plug location in a pressure node of the fundamental longitudinal-acoustic mode.

Because of the excitation of the fundamental longitudinal-acoustic mode, the flame front will oscillate and undergo periodic acceleration at a frequency of ~ 800 Hz. A theory of a periodically accelerated flame front, presented by Markstein,[32] gives predictions of the threshold velocity amplitude which will give rise to an unstable flame front, resulting in a wrinkled or cellular flame and an increased rate of combustion.

For our experiments in air, the laminar flame speed S_u (relative to the unburnt gas) is 40–60 cm/s, and the flame thickness $\mathscr{L}$ is estimated to be in the range of 0.1–1.0 mm. For this parameter range, the fundamental acoustic-mode frequency ($f = 800$ Hz) results in a dimensionless frequency, $\Omega \equiv \pi f \mathscr{L}/S_u$, of 0.4–6.0. For this range the theory presented by Markstein predicts an unstable flame oscillation will result from acoustic oscillations that exceed 4–6 times the laminar flame speed. Since the measured flame propagation speed in the early constant-pressure phase of the combustion obeys $V_f = (T_b/T_u)S_u = 5S_u$ for a flame temperature $T_b = 1500$ K and initial temperature $T_u = 300$ K,[35] this translates into a prediction of an acoustic velocity amplitude V_{01} threshold for instability of $V_{01}^{\text{th}}/V_f = 0.8$–$1.2$. Our experimental values of the threshold for combustion enhancement (Fig. 12 and Table I) are in good agreement with this predicted threshold.

For higher-frequency modes, the velocity amplitude threshold is predicted to increase, so that the acoustic instability in the fundamental longitudinal mode is expected to be most easily excited. This explains why the acoustic instability was invariably observed in this mode.

For the estimated range of flame thickness (0.1–1.0 mm), the vibration-induced instability is predicted to be most easily excited at wavelengths of 0.2–1.0 cm. This wavelength is of the same size as the wrinkles and cellular flame structure visible on the schlieren photographs during e-beam-enhanced combustion.

The agreement with theoretical predictions for the threshold acoustic velocity amplitude and dimensions of the cellular structure provides further evidence that the fluid motion (and associated acceleration) from the fundamental longitudinal-acoustic mode is responsible for the e-beam-enhanced combustion. This agreement also supports the validity of the theory of a periodically accelerated flame front.

VI. SUMMARY

Injection of an electron beam into premixed combustible gases in a closed cylindrical chamber generated large-amplitude acoustic waves. Provided that the velocity amplitude of the fundamental longitudinal-acoustic mode was approximately equal to or greater than the flame propagation speed, the e-beam injection resulted in an increased rate of combustion. The enhanced combustion was characterized by faster flame propagation, increased rates of pressure rise, more rapid rise of OH-line emission, a wrinkled or cellular flame structure, and an increased level of acoustic instability in the fundamental longitudinal mode. This instability was audible as a loud squeak.

The existence of a threshold acoustic velocity amplitude for excitation of the acoustic instability, the occurrence of this instability in the lowest-frequency acoustic mode, the presence of a wrinkled or cellular flame, and the associated increase in combustion rate are consistent with a theoretical model of a periodically accelerated flame. The value of the threshold acoustic velocity amplitude and the dimensions of the cellular structure of the unstable flame fronts are in good numerical agreement with the predictions of this model. This supports the validity of the model and provides strong evidence that excitation of the fundamental longitudinal-acoustic mode by the e-beam injection is the mechanism of combustion enhancement.

ACKNOWLEDGMENTS

We acknowledge valuable interactions with Dr. Jeffrey Sell, Dr. Richard Teets, and Dr. Eric Steinhilper at General Motors Research Laboratories. This research was supported by a National Science Foundation Presidential Young Investigator Award, Grant No. ECS-8351837.

[1] W. Jost, *Explosion and Combustion Processes in Gases* (McGraw-Hill, New York, 1946), p. 508.
[2] P. S. Meyers, O. A. Uyehara, and H. K. Newhall, in *Engine Emissions; Pollutant Formation and Measurement*, edited by G. S. Springer and D. J. Patterson (Plenum, New York, 1973), Chap. 1.
[3] R. G. Adbel-Gayed and D. Bradley, in *Proceedings of the International Conference on Fuel-Air Explosions*, edited by J. H. S. Lee and C.M. Guirao (University of Waterloo, Waterloo, Ontario, 1982), p. 51.
[4] T. M. Sloane and J. W. Ratcliffe, General Motors Research Laboratories Research Publication No. GMR-4404, July 11, 1983.
[5] H. C. Jaggers and A. von Engel, Combust. Flame **16**, 275 (1971).
[6] C. S. Maclatchy, R. M. Clements, and P. R. Smy, Combust. Flame **45**, 161 (1982).
[7] E. G. Groff and M. K. Krage, Combust. Flame **56**, 293 (1984).
[8] J. F. Grant, E. P. Marram, and M. E. McIlwain, Combust. Sci. Technol. **30**, 171 (1983).
[9] P. L. Pitt, J. D. Ridley, and R. M. Clements, Combust. Sci. Technol. **35**, 277 (1984).
[10] R. Hickling and W. R. Smith, Society of Automotive Engineers Paper No. 740114, 1974.
[11] J. A. Sell, General Motors Research Laboratories Research Publication No. GMR-5247, Jan. 9, 1986.
[12] R. M. Gilgenbach, S. W. Bidwell, R. A. Bosch, M. L. Brake, J. E. Tucker, T. E. Repetti, and J. A. Sell, J. Appl. Phys. **62**, 2553 (1987).
[13] R. A. Strehlow, *Fundamentals of Combustion* (Krieger, New York, 1979), Sect. 8.6.

[14]L. D. Horton and R. M. Gilgenbach, Phys. Fluids **25**, 1702 (1982).
[15]M. L. Brake, T. Repetti, K. Pearce, and R. Lucey, J. Appl. Phys. **60**, 99 (1986).
[16]A. G. Gaydon, *The Spectroscopy of Flames* (Wiley, New York, 1957), p. 244.
[17]W. Jost, *Explosion and Combustion Processes in Gases* (McGraw-Hill, New York, 1946), pp. 136–138.
[18]A. G. Gaydon and H. G. Wolfhard, *Flames; Their Structure, Radiation, and Temperature*, 2nd ed. (Chapman and Hall, London, 1960), pp. 224–225.
[19]D. W. Koopman and K. A. Saum, J. Appl. Phys. **44**, 5328 (1973).
[20]D. J. Eckstrom (private communication).
[21]J. M. Meek and J. D. Craggs, *Electrical Breakdown of Gases* (Oxford University, London, 1953), pp. 51–52.
[22]Ye V. Stupochenko, S. A. Losev, and A. I. Osipov, *Relaxation in Shock Waves* (Springer, New York, 1967), Chap. 1.
[23]A. C. Tam, Rev. Mod. Phys. **58**, 381 (1986).
[24]R. W. B. Stephens and A. E. Bate, *Acoustics and Vibrational Physics*, 2nd ed. (St. Martin's, New York, 1966), p. 386.
[25]L. L. Beranek, *Acoustics*, 2nd ed. (American Institute of Physics, New York, 1986), p. 40.
[26]R. A. Bosch, S. W. Bidwell, and R. M. Gilgenbach, IEEE Trans. Plasma Sci. **PS-16**, 428 (1988).
[27]N. A. Krall and A. W. Trivelpiece, *Principles of Plasma Physics* (San Francisco Press, San Francisco, 1986), pp. 319–321.
[28]D. J. Eckstrom and H. C. Walker, Jr., J. Appl. Phys. **51**, 2458 (1980).
[29]H. E. White and D. H. White, *Physics and Music; The Science of Musical Sound* (Saunders College, Philadelphia, 1980), pp. 352, 413.
[30]G. H. Markstein, in *Fourth Symposium (International) on Combustion* (Williams and Wilkins, Baltimore, 1953), p. 44.
[31]G. H. Markstein and L. M. Somers, in *Fourth Symposium (International) on Combustion* (Williams and Wilkins, Baltimore, 1953), p. 527.
[32]G. H. Markstein, in *Nonsteady Flame Propagation*, edited by G. H. Markstein (MacMillan, New York, 1964), pp. 52–58.
[33]D. E. Kooker, Combust. Flame **49**, 141 (1983).
[34]J. F. Clarke, in *The Mathematics of Combustion*, edited by J. D. Buckmaster (SIAM, Philadelphia, 1985), Chap. V.
[35]K. K. Kuo, *Principles of Combustion* (Wiley, New York, 1986) p. 320.